Seasonal Prediction Skills in the CAMS-CSM Climate Forecast System

Bo Liu

State Key Laboratory of Severe Weather

Jingzhi SU (✉ sujz@cma.gov.cn)

State Key Laboratory of Severe Weather

Libin MA

State Key Laboratory of Severe Weather

Yanli TANG

State Key Laboratory of Severe Weather

Xinyao RONG

State Key Laboratory of Severe Weather

Jian LI

State Key Laboratory of Severe Weather

Haoming CHEN

State Key Laboratory of Severe Weather

Boqi LIU

State Key Laboratory of Severe Weather

Lijuan HUA

State Key Laboratory of Severe Weather

Renguang WU

Institute of Atmospheric Physics Chinese Academy of Sciences

Research Article

Abstract

The seasonal predictability in the CAMS-CSM climate forecast system is evaluated with a set of retrospective forecast experiments during the period of 1981-2019. The CAMS-CSM, which has been registered for the sixth phase of the coupled model intercomparison project (CMIP6), is an atmosphere-ocean-land-sea ice fully coupled general model. The assimilation scheme used in the forecast system is the 3-dimentional nudging, including both the atmospheric and oceanic components.

The analyses mainly focus on the seasonal predictable skill of sea surface temperature, 2-m air temperature, and precipitation anomalies. The analyses revealed that the model shows a good prediction skill for the SST anomalies, especially in the tropical Pacific, such as El Niño-Southern Oscillation (ENSO) events. The anomaly correlation coefficient (ACC) score for ENSO can reach 0.75 at 6-month lead time. Furthermore, the extreme warm/cold Indian Ocean dipole (IOD) events are successfully predicted at 3- and even 6-month lead times. The whole ACC of IOD events between the observation and the prediction can reach 0.51 at 2-month lead time. There are reliable seasonal prediction skills for 2-m air temperature anomalies over most of the Northern Hemisphere, where the correlation is mainly above 0.4 at 2-month lead time, especially over the East Asia, North America and South America. However, the seasonal prediction for precipitation still faces a big challenge. The source of precipitation predictability over the East Asia can be partly related to strong ENSO events. Additionally, the anomalous anticyclone over the western North Pacific (WPAC) which connects the ENSO events and the East Asian summer monsoon (EASM) can be well predicted at 6-month lead time.

1. Introduction

Climate events on seasonal time scales are essentially related to social economy and people's living life. Hence, how to get accurate seasonal forecast has always been an important issue. The prediction methods can be generally divided into two types (Graham 1987; Jin et al. 2008; Tang et al. 2018): the statistical models (Graham 1987; Ren et al. 2018) and the dynamic models (Jin et al. 2008; Kirtman 2003; Luo et al. 2005; Zhu et al. 2017). Over the past decades, benefited from advances in climate system models (CSMs) and the improvements in observation network, such as the Tropical Atmosphere Ocean (TAO) program conducted since the 1980s (McPhaden 1995) and the Tropical Ocean-Global Atmosphere (TOGA) program during 1985–1994, the dynamical seasonal prediction has achieved great progresses. Many operational and scientific centers have established seasonal climate prediction system based on dynamical methods (Becker et al. 2014; Johnson et al. 2019; Liu et al. 2015; Molteni et al. 2011; Saha et al. 2006).

In addition to the inherent performance of CSMs, the dynamical seasonal prediction skill, on a certain extent, is dependent on the data assimilation system (Chen et al. 1997; Jin et al. 2008; Moore and Kleeman 1996; Moore et al. 2006). Unlike the predictable source of the traditional weather forecast within about 10 days, which mainly comes from the atmospheric initial conditions, the predictable source of seasonal, or even longer time period, forecasts mainly is attributed to the slow-varying processes of the

climate system, which is largely resided in the ocean memory. Thus, the ocean initialization plays a vital role in the seasonal forecast system.

To obtain accurate ocean initiation conditions (ICs), a variety of data assimilation methods have been developed to assimilate the ocean observations, including the real-time in situ observations and the satellite products (Balmaseda et al. 2013; Behringer and Xue 2004). The relatively advanced and sophisticated data assimilation schemes include the optimal interpolation (OI) (Gandin 1965), the 3-dimensional variational method (3D-Var) (Lorenc 1986), the 4-dimensional variational method (4D-Var) (Sugiura et al. 2008), and the ensemble Kalman filter (EnKF) (Evensen 1994; Liu et al. 2004; Zhang et al. 2007). By assimilating the sea surface temperature (SST) data into a hybrid coupled model (HCM) model using a 3D-Var method, significant improvement could be obtained for ENSO prediction, especially at the 4-month lead time (Tang et al. (2003). The 4D-Var is considered to be more physically consistent. Sugiura et al. (2008) applied the 4D-Var initialization approach to obtain a successful prediction of the 1997/98 El Niño event up to 1.5-year lead time. However, since the physical processes and parameterizations are different among the CSMs, the assimilation scheme used in a CSM cannot be directly applied to the others (Tang et al. 2003). Furthermore, although the complex assimilation scheme might obtain a better initial fields, the computational cost could be a major concern when these approaches are applied to high-resolution coupled models, and thus further scientific and technical efforts are still required (Small et al. 2014).

A more economic and practical approach in assimilation is the Newtonian relaxation (nudging) approach, in which the model initial fields are nudged towards the observation or reanalysis with restore coefficients. One of the most widely used nudging schemes is the SST nudging, namely nudging towards the observed SST (Keenlyside et al. 2016; Luo et al. 2005; Luo et al. 2008; Zhu et al. 2017) or SST anomalies (Chen et al. 2004; Ren and Nie 2020). The mechanism for SST-nudging scheme is that not only the realistic temperature in the mixed layer can be reproduced, but also the observed variability of the subsurface temperature can be partially obtained owing to the air-sea interaction and coupling (Keenlyside et al. 2005; Kumar and Zhu 2018; Luo et al. 2005; Wang et al. 2019). Therefore, this scheme is more suitable for the area where air-sea interaction is strong, such as the tropical Pacific. By implementing the SST nudging scheme into the SINTEX-F, Luo et al. (2005) achieved a remarkable extended ENSO prediction skill up to 2-years lead time. In order to have substantial skill on other atmospheric variables, such as air temperature and precipitation, more observed data might need to be assimilated as well. Baehr et al. (2014) reproduced the observed surface temperature anomalies at 2−4 months lead time, especially in the tropics, based on the initialization of atmospheric, oceanic and sea ice components of the MPI-ESM climate model with a full field nudging technology.

Recently, a state-of-the-art model, called CAMS-CSM, is developed by the Chinese Academy of Meteorological Sciences (CAMS), which is fully coupled with atmosphere-ocean-land-sea ice components (Rong et al. 2018). The CAMS-CSM has been registered for the sixth phase of the coupled model intercomparison project (CMIP6) (Eyring et al. 2016; Rong et al. 2020) and shown good simulation performance on climatological mean states, seasonal cycles, and major climate variability modes

including Madden-Julian Oscillation and ENSO in pre-industrial and historical experiments (Hua et al. 2019; Rong et al. 2018). The purpose of this study is to document a new climate forecast system based on the CAMS-CSM model, which is initialized with both the atmospheric and oceanic components. For the analysis of predictive skill, the analyses mainly focus on the SST, but other variables will be briefly discussed as well.

The rest of this paper is arranged as follows. The climate model, experimental designs, data and methods are introduced in Sect. 2. The performance of the seasonal climate forecast system is evaluated in Sect. 3, including the SST, 2-m air temperature and precipitation anomalies, and climate anomalies related to ENSO over the East Asia-Western North Pacific (EA-WNP) in the ENSO decaying summer. Conclusion and discussion are included in the Sect. 4.

2. The Climate Model, Hindcast Experiments And Data

2.1 The CAMS-CSM Climate Model

The forecast system is based on the CAMS-CSM (Rong et al. 2018), which was developed at the CAMS. The atmospheric component of CAMS-CSM is a modified version of ECHAM5.4 (Roeckner et al. 2003). It is configured by the T106L31 resolution, with a 1° resolution in horizontal direction and 31 vertical layers extending from surface to 10 hPa. The modifications mainly include a Two-step Shape Preserving Advection Scheme (TSPAS) for passive tracer transport (Yu 1994) and k-distribution scheme for radiation transfer parameterization (Zhang et al. 2006a; Zhang et al. 2006b). The oceanic component is the Modular Ocean Model version 4 (MOM4) (Griffies et al. 2004), which is configured by a resolution of about 1°×1° in zonal and meridional directions and 50 vertical layers. The atmospheric and oceanic components are coupled by the GFDL Flexible Modeling System (FMS) coupler. Moreover, the land model named CoLM (Dai et al. 2003) is included in the atmospheric component, and a five-layer sea-ice model (SIS) is included in MOM4 (Winton 2000). More details on the model description can be referred to Rong et al. (2018).

2.2 Design of the CAMS-CSM hindcast experiments

The nudging initialization scheme is achieved by adding a Newtonian damping term into the prognostic equations, resulting in the model fields adjusted towards observations. In this study, both the atmospheric and oceanic ICs are constructed by the 3-dimensional nudging technology. For the atmospheric initial conditions, the 6-hourly air temperature, relative humidity, the surface pressure, zonal and meridional winds from the 55-year Japanese Reanalysis Project (JRA55) atmospheric reanalysis data (Kobayashi et al. 2015) are assimilated with a restoring time scale of 0.5 days. For the oceanic initial conditions, the pentad temperature and salinity above 1000 m from the National Center for Atmospheric Research (NCEP) GODAS ocean reanalysis data (Behringer and Xue 2004) are assimilated in the global ocean south of 60°N. The restoring time scale is set at 5 days near the equator and gradually increased to 30 days outside of 40°N/S. Eight ensemble simulations have been conducted to calibrate and evaluate the prediction skills, starting once a month from January 1980 to December 2019. The 6-month predictions

with initial conditions (ICs) at 0000, 0600, 1200, and 1800 UTC were made on the 20th and 21th of every month. Daily mean data were stored for the several (8–11) days in the initial incomplete month, and they were not used to calculate monthly mean. The following prediction month is the so-called the "month lead time". For example, the prediction at 1-month lead time from January initiation conditions is the forecast for February. In order to make the different initial periods comparable, the 39-year prediction period from January 1981-December 2019 are analyzed for all the lead times. These 8 runs from the hindcasts form the ensemble that is used for calibration and skill assessment of seasonal predictions.

2.3 Data and methods

The verification data used in this paper include the SST, precipitation, 2-m air temperature and 850-hPa wind. The global observed monthly SST dataset is the Extended Reconstructed Sea Surface Temperature (ERSST v5) dataset with 2°⊆2° resolution (Huang et al. 2017). The precipitation, 2-m air temperature and 850-hPa wind data are from the 55-year Japanese Reanalysis Project (JRA-55) (Kobayashi et al. 2015). All the above reanalysis/observations cover a 39-yr period from 1981−2019 and are interpolated onto the CASM-CSM model grid. The anomalies of each variable are calculated relative to 1981−2010 climatology. The statistical methods include regression, correlation and physical analysis, and the standard two-tailed Student's *t* test is used to estimate the significant levels. The anomaly correlation coefficient (ACC) and root-mean-square error (RMSE) between the predicted and the observations are used as measures of the prediction skill.

3. Results

3.1 Global SST anomalies

The global distributions of prediction correlation skill of SST anomalies between the observation and predictions are shown in Fig. 1 for 1-, 3- and 6-month lead times during the period 1981−2019. The result shows a high prediction skill of SST at 1-month lead time with large ACC value, higher than 0.6 over the tropics and mid-latitudes oceans (Fig. 1a). The highest predictability appears in the central and eastern equatorial Pacific where correlation skill is above 0.9. The model shows high predictability (ACC > 0.6) in most regions of the Pacific at 3-month lead time (Fig. 1b). High ACC is still seen in the western tropical Atlantic. At 6-month lead time, the domain of significant SST predictabilities is mostly found in the central tropic Pacific (Fig. 1c). The predictability becomes weak over the tropical Indian and western tropical Atlantic Ocean. The prediction skills of SST anomalies at 6-month lead time in the CAMS-CSM forecast system are quite comparable with most models from the North American Multi-model Ensemble (NMME) project (Zhu et al., 2017).

In order to understand more details about the seasonal predictability of global SST, a view of seasonal difference in anomalous SST prediction skills from different initial times are examined for the lead times of 3 and 6 months (Fig. 2 and Fig. 3), respectively. For these two lead times, the upmost prediction skill of SST anomalies is still over the tropical central and eastern Pacific where the correlation is above 0.6 for nearly all starting months. Comparing the predictability at different starting times, the most skillful

prediction is that initiated from July and October, with the correlation in the tropical central Pacific up to 0.9 at 3-month lead time (Fig. 2d) and remaining above 0.7 at 6-month lead time (Fig. 3d). The highest correlation (ACC > 0.8) appears for the initiation starting from July at the 6-month lead time (Fig. 3c), indicating the high predictability of SST in winter. As the lead time increases, the corresponding correlation gradually decreased in other oceanic areas. Nonetheless, there are still some significant predictability in the tropical Indian and tropical Atlantic Ocean basins at 6-month lead time. Owing to the influence of ENSO, the SST warming event over these two regions tends to occur 4–5 months after the mature phases of ENSO events, leading to the better predictability starting on October over the north tropical Indian Ocean and tropical Atlantic Ocean (Fig. 3d). In general, ENSO teleconnections might play an important role in the predictability of SST anomalies in the tropical Indian and Atlantic Ocean. In addition, the Southern Pacific Ocean has the best predictability (ACC > 0.6) in spring and summer for prediction that starts from January and July at 3-month lead times (Figs. 2a and 2c). Guan et al. (2014) had attributed the main reason to the effect of ENSO remote forcing.

3.2 The 2-m air temperature and precipitation anomalies

The seasonal predictabilities of 2-m air temperature and precipitation anomalies are also evaluated for all four seasons (MAM, JJA, SON, DJF respectively represent boreal spring, boreal summer, boreal autumn and boreal winter) (Fig. 4 and Fig. 5). Although the prediction skill of the 2-m air temperature over land is much lower than that of SST, there are significant high correlations during each season in the tropics (Fig. 4), such as the South America, the southern North America, the Maritime Continent, Australia and Africa, with a correlation skill larger than 0.4 at 2-month lead time. The maximum correlation (> 0.7) center appears in the northern South America during MAM (Fig. 4a) and DJF (Fig. 4d). Moreover, the prediction skill seems strongly dependent on regions. For instance, the prediction skill in the central Australia, especially for DJF, is obviously lower than the other places of the Southern Hemisphere, such as Brazil. Over the mid-latitude of the Northern Hemisphere, there is significant prediction skill in the East Asia where the correlation reaches above 0.4 during JJA (Fig. 4b) and SON (Fig. 4c) at 2-month lead time. The northern North America shows significant prediction skill of the 2-m air temperature in JJA and DJF, while prediction skill is weak in SON and DJF over the high-latitude Eurasia.

The prediction of precipitation over land at 2-month lead time (Fig. 5) seems much more difficult than that for SST and 2-m air temperature. The precipitation predictability in the Northern Hemisphere mainly lies in the Middle East, the southeast China, the western and eastern North America where the correlation skill is mainly above 0.2 during DJF (Fig. 5d). The predictability of precipitation seems better in the Southern Hemisphere. There are reliable prediction skills in the southeast Australia and most regions of Brazil, where the correlation skill can reach above 0.6 in some areas during SON and DJF.

3.3 ENSO events

ENSO is a dominant mode on inter-annual timescale in the Pacific Ocean. Many previous studies have shown that the seasonal cycle of the equatorial Pacific SST plays an important role in the development of El Niño events (Guilyardi 2006; Latif et al. 2001). Hence, the seasonal cycle of SST deviation from

annual mean over the equatorial Pacific in model predictions at 1-, 3- and 6-month lead times are compared with the observations (Fig. 6). The predictions at all the three lead times generally are matched well with the observations, including the semi-annual cycle and annual cycle in the western and eastern tropical Pacific, respectively. The two main discrepancies appear in the westward propagation and magnitude of SST deviations. In short lead time (Fig. 6b), the evolution of annual cycle shows a closer match to the observations, with the positive (negative) SST deviations extending westward to around 160°W (130°W), although the magnitude is relatively smaller in the model prediction. The problem of "too westward propagation and too strong" occurs at both 3- and 6-month lead times (Figs. 6c and 6d), which could lead to the lower decaying speed of ENSO events and in turn might lead to the seasonal climate prediction biases in the ENSO decaying phase. This situation will be discussed in the Sect. 3.5.

In an ensemble forecast system, the reasonableness of samples might largely reduce the uncertainty and improve the accuracy of prediction. Previous studies have investigated the relationship between the spread and magnitude of ENSO events in an ensemble prediction (Hu and Kumar 2014; Tang et al. 2008). The Niño3.4 index, which is computed by averaging the anomalous SSTs over the domain of 5°S-5°N, 120°-170°W, is used to represent the ENSO events. The scatterplot between the multi-sample of hindcasts for the DJF Niño3.4 index (x axis) and the spread of ensemble members from different ICs (y-axis) with six lead times is shown in Fig. 7. The spread (y-axis) is taken the absolute value of the difference between each sample and the ensemble mean, and it can be treated as the uncertainty of Niño3.4 index. Firstly, the variance of Niño3.4 index's spread varies with the lead time. The spread, which represents the uncertainty of prediction, becomes bigger with increasing lead time. The spread concentrates within 0.2°C at the 1-month lead time, but it grows up with a wide distribution between 0-0.8°C at 6-month lead time. Secondly, the amplitude of spread increases as the lead time increases. This phenomenon is quite similar to the results based on CFSv2 for ENSO prediction (Hu and Kumar 2014). Compared to the value of total mean of spread (about 0.3°C), the amplitude of Niño3.4 index (about 3°C) is about ten times bigger. In other words, the variance of uncertainty is a smaller amount than that of amplitude, consistent with previous studies (Hu and Kumar 2014; Tang et al. 2008). All the above analysis demonstrates the reasonable spread range of the Niño3.4 index prediction.

The time series of Niño3.4 index during the period of 1981−2019 based on the ERSSTv5 observation and model prediction at 1-, 3- and 6-month lead times are compared to inspect the ENSO prediction skill (Fig. 8a). All of them have been smoothed by 3-month running mean. The results show that the ENSO during most periods can be well predicted at each lead time. The standard deviation of interannual Niño3.4 index at each lead time is around 0.95 °C, which matches well with the observation (0.98 °C). The three strongest El Niño events (1982/83, 1997/98 and 2015/16) can be successfully predicted at 6-month lead time, but the amplitudes are slightly smaller than the observations. Moreover, the stronger La Niña events, such as 1988/89, 1998/99, 2000/01, and 2011/12, can also be successfully predicted at 6-month lead time, and the predicted amplitudes are very close to the observations. However, the biases and uncertainties become much bigger for the weaker ENSO or neutral events.

ENSO prediction has a "spring barrier" feature both in observations and models (Latif et al. 1994; Tang et al. 2018), which means the predicted skill of ENSO decreases rapidly during spring season. It is clear that the intrinsic "spring barrier" situation also exists in the CAMS-CSM climate forecast system (Figs. 8b and 8c). A significant lower center of ACC (< 0.75) lies from January to April at 3–6 months lead time (Fig. 8b), while a higher center of ACC (> 0.95) exists from July to December at 1–3 months lead time, corresponding with the higher (> 0.65 ℃) and lower (< 0.3 ℃) RMSE center respectively (Fig. 8c). The predicted skill in spring at 6-month lead time can reaches 0.7, which is comparable with the performance in SINTEX-F (Luo et al., 2005). Some researches demonstrated that the spring barrier came from the phase locking of ENSO to the seasonal cycle (Wu et al. 2009). During the springtime, the phase transition of ENSO results in a low signal-to-noise ratio (Xue et al. 1994). Some researches emphasized the lower variance of anomalous SST in spring (Fan et al. 2000). Although lots of effort have been made to reduce the spring prediction barrier, this defect still exists in the state-of-art climate models (Becker et al. 2014; Luo et al. 2005; Zhu et al. 2017). However, this forecast system still shows highly credibility to ENSO prediction at 6-month lead time, with the ACC of Niño3.4 index reaching about 0.88 and 0.75 at 3- and 6-month lead times, respectively (Fig. 9a). The RMSE (about 0.63 ℃) of Niño3.4 index at 6-month lead time is much lower than one standard deviation of 0.98 ℃ (Fig. 9b).

ENSO has a great impact on other basins, such as the Southeast Indian Ocean and the tropical Atlantic. Hence, the correlation and the RMSE are calculated for different indices from the Pacific, Indian and Atlantic Ocean at each lead month between the observation and the prediction (Fig. 9). The result shows that there is a certain degree of predictability for these three basins. The most skillful area lies in the central and eastern Pacific Ocean. The skill (either correlation or RMSE) of the index over the Pacific Ocean, especially the Niño3.4 index, is better than those in the other ocean regions. In the Indian Ocean, the Eastern Indian Ocean (EIO) index (averaged SST anomalies in the domain of 90°-110°E, 10°S-0°), decreases rapidly from 0.72 at 1-month lead time to around 0.55 at 3-month lead time, with little predictability after 3-month lead time informed by declined correlation and increased RMSE. The predictability of the South Indian Ocean (SIO) index remains significant at 6-month lead time, with correlation skill (about 0.72) slightly larger than that (about 0.7) at 4-month lead time. This might be related to the lagged influence of ENSO. Another region which is largely affected by ENSO is tropical Atlantic, represented by the ATL index (averaged 60°-40°W, 10°-20°N) here. The model shows certain predictability of ATL index with ACC from 0.85 at 1-month lead time deceasing to around 0.6 at 6-month lead time, which are somewhat higher than those for the SIO index.

3.4 The Indian Ocean Dipole

The Indian Ocean Dipole (IOD) has significant impacts on East Asian and Western North Pacific (EA-WNP) climate (Ashok et al. 2004; Jiang et al. 2019; Nur'utami and Hidayat 2016; Xu and Guan 2017). Although it is still a great challenge to predict the IOD, the extreme warm/cold IOD events (e.g., 1995, 1998, 1999 and 2017) are well predicted at 3-month, even at 6-month lead time (Fig. 10a). Similar to the ENSO prediction, the prediction of IOD events is also difficult in spring, but it seems that the prediction barrier appears earlier. The IOD prediction skill at the 2-month lead time rapidly decreases from around

0.6 during winter time to 0.2 in spring. The RMSE at 6-month lead time has the highest value during spring. Meanwhile the prediction skill is still low in autumn and winter. However, the predictability of IOD index is higher starting from May to December at 1 to 3-month lead time. In particular, when the initial time starts from summer, the correlation skill of the IOD index reaches up to 0.5 at 5-month lead time. The ACC of IOD events between the prediction and the observation is 0.64, 0.51 and 0.35 at 1-, 2- and 3-month lead times, respectively, indicating a rapid decrease of prediction skill after 2-month lead time. The prediction skill of IOD is comparable with the BCC_CSM1.1 climate model (Liu et al. 2015).

3.5 Predictability over EA-WNP related to ENSO

3.5.1 SST anomalies in El Niño decaying summer

One of most dominant climate systems in EA-WNP is the East Asian Summer Monsoon (EASM), and its variability has great impacts on social and economic influences. Many researches have shown that one of the most important factors affecting the EASM is the ENSO (Chen et al. 1992; Wang et al. 2000; Zhang et al. 1999). The impacts of ENSO on the EASM is not direct, and the anomalous anticyclone over the western North Pacific (WPAC) in the ENSO decaying summer (June to August; JJA(1)) plays a bridge role connecting the ENSO and the EASM (Wu et al. 2009; Wu and Kirtman 2003; Xie et al. 2009; Yang et al. 2007). Therefore, for the successful prediction over the EASM, the WPAC and SST anomalies over the Indo-western Pacific are two important prerequisite factors.

The regressions of JJA(1) SST anomalies on the normalized previous DJF Niño3.4 index are shown in Fig. 11. In the observation (Fig. 11a), there are significant warming centers over the tropical Indian Ocean, the South China Sea, and the East China Sea. The distribution of SST anomalies in the Indo-western Pacific is quite similar to the observations in the decaying summer of El Niño events at all leading times. The bias at 1-month lead time lies in the overestimated amplitude in the Indian Ocean and South China Sea (Fig. 11b). In addition, the warming area in the western tropical Pacific seems to slightly shift westward compared with the observation. At 3-month lead time, the prediction is quite close to the observation in the Indian Ocean where the overestimated warming has been slightly reduced (Fig. 11c). The bias over the western North Pacific Ocean becomes bigger. When initiated with 6-month lead time, the warming pattern is much closer to the observations in the South Indian Ocean. However, the warming in the South China Sea is weaker than that in the observations (Fig. 11d). The bias seems to become even bigger with the lead time increase in the tropical western Pacific. This might be a common bias in climate models with the speed of ENSO decaying slower than the observations, a reason that may come from the model systematic errors in the simulation of the cold togue (Jiang et al. 2017; Tao et al. 2015).

3.5.2 Precipitation and Circulation Anomalies in El Niño decaying summer

The successful prediction on precipitation beyond 1- or 2-month lead time is very difficult in current climate models. Since the ENSO and its decaying summer SSTA can be reasonably predicted at a quite

long-term period, their relationship could be used to make the predictability of precipitation more available (Liu et al. 2017; Shi and Wang 2018). Figure 12 shows the regression of JJA(1) precipitation and 850-hPa wind anomalies at various lead times on DJF Niño3.4 index over the Indian Ocean and western North Pacific. In the observations, the WPAC is obviously found over the western North Pacific. Affected by the Pacific-Japan teleconnection, the precipitation anomalies display a distinct triple meridional structure over the EA-WNP (Fig. 12a). One positive anomalous rain band is found on its northwest and north flank of the WPAC from the South China to the South of Japan after the El Niño events, which matches with the area covered by the Mei-Yu band. Another positive rain band lies over the North Indian Ocean to the Maritime Continent, owing to anomalous winds that enhance the prevailing trade during summertime. These characters are well predicted by the CAMS-CSM forecast system (Fig. 12b-12d), especially at 1- and 3-month lead times. The prediction bias at 1-month lead time is mainly because the predicted WPAC is a little bit stronger and shifts westward than the observed (Fig. 12b), resulting in much weaker moisture from the tropical Pacific to land over southern China and also weaker positive rainfall over South China. At the 3-month lead time, the amplitude of predicted WAPC is weakened, leading to reduced easterly anomalies on south flank of the WPAC (Fig. 12c). Besides, the positive rainfall anomalies over the South Indian Ocean are much weaker than the observations. When the prediction is initiated at 6-month lead time, the WPAC can still be successfully predicted but much weaker, resulting in weaker rainfall anomalies over the East Asia. Anyway, the south branch of positive rainfall anomalies over the North Indian Ocean to the South China Sea are successfully predicted at 6-month lead time (Fig. 12d).

4. Conclusion And Discussion

The seasonal predictability for the period of 1981–2019 based on the CAMS-CSM climate forecast system has been evaluated. The forecast system includes a 3-dimentional nudging initialization scheme which assimilates atmospheric and oceanic data, and eight ensemble members per month were carried out with a lead time up to 6 months. From the analysis of Niño3.4 index, all the El Niño events, including the top three strongest 1982/83, 1997/98, and 2015/16, and La Niña events can be predicted successfully at 6-month lead time. The ACC skill of Niño3.4 index can reach 0.75 at 6-month lead time, which is comparable to current numerous dynamic seasonal forecast systems. However, the predicted magnitudes for some particular El Niño (La Niña) events at 6-month lead time are weaker (larger) than the observed. The largest predictability over the Pacific is prediction starting from July at both 3- and 6-month lead times. The results also indicate the prediction skills not only have seasonal dependence, but also significant difference among the ocean basins.

As far as the IOD events, the extreme warm/cold IOD events, (e.g., 1997, 1998, 2007 and 2017) are successfully predicted at 3-month and even at 6-month lead times. The IOD events has the highest predictability for predictions starting from summertime, which remains up to 5-month lead time. Generally, a certain degree of predictability skill exists on IOD events, with a lead time up to 2 months in advance. The ACC of IOD events between the observation and the prediction can reach 0.51 at 2-month lead time.

For the prediction of 2-m air temperature over land, the prediction skill is much lower than that of SST. The seasonal prediction skills over land are largely dependent upon the initial time. The prediction starting from April and July, has reliable skill at 2-month lead time over most areas of the North Hemisphere where the correlation is mainly above 0.4, especially over the North America and the East Asia.

The prediction on the spatial patterns of SST, precipitation and circulation anomalies in ENSO decaying summer are also evaluated. The forecast system can well predict the pattern and magnitude of SSTA over the EA-WNP at 6-month lead time, especially the Indo-Pacific warming. The bias seems to become bigger over the tropical western Pacific with the lead time increase. This might be a common bias in the present coupled models, in which the speed of ENSO decaying is slower than observation. The positive rainfall related to ENSO events over the Mei-Yu region can be well predicted at 3-month lead time, owing to that the ENSO-related WPAC can be predicted at a long-term period.

The reasonable predictability of the results obtained in this paper may mainly benefit from two parts. First is the realistic simulation of the CAMS-CSM on the climatology and ENSO evolution over the tropical Pacific (Rong et al. 2018). Another is the data assimilation scheme. Compared to sophisticated ones, the simple nudging scheme is competent for the seasonal prediction both in skill score and efficiency. Meanwhile, assimilating more observed data (including 3-dimentional atmospheric and oceanic variables) here may enable the extreme events, such as the unusual ENSO events in 2015/2016 (Su et al. 2018; Zhong et al. 2019), to be successfully predicted at 6-month lead time. By participating in the (Chinese) multi-model ensemble project, it will help to improve the seasonal climate prediction skills, as many reasonable results have already been obtained in the CAMS-CSM forecast system. The present achievements also lay a foundation for setting up a seamless weather-climate prediction system in the future.

Declarations

References

Ashok K, Guan ZY, Saji NH, Yamagata T (2004) Individual and combined influences of ENSO and the Indian Ocean Dipole on the Indian summer monsoon Journal of Climate 17:3141-3155 doi:Doi 10.1175/1520-0442(2004)017<3141:Iacioe>2.0.Co;2

Baehr J et al. (2014) The prediction of surface temperature in the new seasonal prediction system based on the MPI-ESM coupled climate model Climate Dynamics 44:2723-2735 doi:10.1007/s00382-014-2399-7

Balmaseda M, Mogensen K, Weaver A (2013) Evaluation of the ECMWF ocean reanalysis ORAS4 Quarterly Journal of the Royal Meteorological Society 139:1132–1161

Becker E et al. (2014) The NCEP Climate Forecast System Version 2 Journal of Climate 27:2185-2208 doi:10.1175/jcli-d-12-00823.1

Behringer DW, Xue Y (2004) Eighth Symposium on Integrated Observing and Assimilation Systems for Atmosphere, Oceans, and Land Surface, AMS 84th Annual Meeting, Washington State Convention and Trade Center, Seattle, Washington Am Meteor Soc 23:11-15

Chen DK, Cane M, Kaplan A, Zebiak S, Huang D (2004) Predictability of El Niño over the past 148 years Nature 428:733-736

Chen DK, Zebiak SE, Cane MA, Busalacchi AJ (1997) Initialization and predictability of a coupled ENSO forecast model. Monthly Weather Review 125

Chen L, Dong M, Shao Y (1992) The Characteristics of Interannual Variations on the East Asian Monsoon Journal of the Meteorological Society of Japan Ser II 70:397-421 doi:10.2151/jmsj1965.70.1B_397

Dai YJ et al. (2003) The Common Land Model Bulletin of the American Meteorological Society 84:1013-1023 doi:10.1175/Bams-84-8-1013

Evensen G (1994) Sequential data assimilation with a nonlinear quasigeostrophic model using Monte Carlo methods to forecast error statistics Journal of Geophysical Research 99:10143–10162

Eyring V, Bony S, Meehl GA, Senior CA, Stevens B, Stouffer RJ, Taylor KE (2016) Overview of the Coupled Model Intercomparison Project Phase 6 (CMIP6) experimental design and organization Geoscientific Model Development 9:1937-1958 doi:10.5194/gmd-9-1937-2016

Fan Y, Allen MR, Anderson DLT, Balmaseda MA (2000) How Predictability Depends on the Nature of Uncertainty in Initial Conditions in a Coupled Model of ENSO Journal of Climate 13:3298-3313 doi:10.1175/1520-0442(2000)013<3298:Hpdotn>2.0.Co;2

Gandin L (1965) Objective analysis of meteorological fields US Dept Commerce and National Science Foundation Washington, DC (Original in Russian, ob"ektivnyi analiz meteorologicheskikh polei, 1963)

Graham NEM, J. Barnett, T. P. (1987) An investigation of the El Nin˜o-Southern Oscillation cycle with statistical models: II. Model results Journal of Geophysical Research 92:14271-14289

Griffies SM, Harrison MJ, Pacanowski PC (2004) A Technical Guide to MOM4 GFDL Ocean Group Technical Report NO 5, Princeton, NJ, NOAA/Geophysical Fluid Dynamics Laboratory:339pp

Guilyardi E (2006) El Niño–mean state–seasonal cycle interactions in a multi-model ensemble Climate Dynamics 26:329-348 doi:10.1007/s00382-005-0084-6

Hu Z-Z, Kumar A (2014) How Variable Is the Uncertainty in ENSO Sea Surface Temperature Prediction? Journal of Climate 27:2779-2788 doi:10.1175/jcli-d-13-00576.1

Hua LJ, Chen L, Rong XY, Li J, Zhang G, Wang L (2019) An Assessment of ENSO Stability in CAMS Climate System Model Simulations Journal of Meteorological Research 33:80-88 doi:10.1007/s13351-018-8092-8

Huang BY et al. (2017) Extended Reconstructed Sea Surface Temperature, Version 5 (ERSSTv5): Upgrades, Validations, and Intercomparisons Journal of Climate 30:8179-8205 doi:10.1175/Jcli-D-16-0836.1

Jiang W, Huang G, Hu K, Wu R, Gong H, Chen X, Tao W (2017) Diverse Relationship between ENSO and the Northwest Pacific Summer Climate among CMIP5 Models: Dependence on the ENSO Decay Pace Journal of Climate 30:109-127 doi:10.1175/jcli-d-16-0365.1

Jiang X, Zhang T, Tam CY, Chen J, Lau NC, Yang S, Wang Z (2019) Impacts of ENSO and IOD on Snow Depth Over the Tibetan Plateau: Roles of Convections Over the Western North Pacific and Indian Ocean Journal of Geophysical Research: Atmospheres 124:11961-11975 doi:10.1029/2019jd031384

Jin EK et al. (2008) Current status of ENSO prediction skill in coupled ocean–atmosphere models Climate Dynamics 31:647-664 doi:10.1007/s00382-008-0397-3

Johnson SJ et al. (2019) SEAS5: the new ECMWF seasonal forecast system Geoscientific Model Development 12:1087-1117 doi:10.5194/gmd-12-1087-2019

Keenlyside N, Latif M, Botzet M, Jungclaus J, Schulzweida U (2016) A coupled method for initializing El Niño Southern Oscillation forecasts using sea surface temperature Tellus A: Dynamic Meteorology and Oceanography 57:340-356 doi:10.3402/tellusa.v57i3.14661

Keenlyside N, Latif M, Botzet M, Jungclaus J, Schulzweida UWE (2005) A coupled method for initializing El Nino Southern Oscillation forecasts using sea surface temperature Tellus A 57:340-356 doi:10.1111/j.1600-0870.2005.00107.x

Kirtman BP (2003) The COLA anomaly coupled model: ensemble ENSO prediction Monthly Weather Review 131

Kobayashi S et al. (2015) The JRA-55 Reanalysis: General Specifications and Basic Characteristics Journal of the Meteorological Society of Japan Ser II 93:5-48 doi:10.2151/jmsj.2015-001

Kumar A, Zhu J (2018) Spatial Variability in Seasonal Prediction Skill of SSTs: Inherent Predictability or Forecast Errors? Journal of Climate 31:613-621 doi:10.1175/jcli-d-17-0279.1

Latif M et al. (1994) A review of ENSO prediction studies Climate Dynamics 9:167-179 doi:10.1007/bf00208250

Latif M et al. (2001) ENSIP: the El Niño simulation intercomparison project Climate Dynamics 18:255-276 doi:10.1007/s003820100174

Liu B, Huang G, Hu K, Wu R, Gong H, Wang P, Zhao G (2017) The multidecadal variations of the interannual relationship between the East Asian summer monsoon and ENSO in a coupled model Climate Dynamics 51:1671-1686 doi:10.1007/s00382-017-3976-3

Liu XW et al. (2015) Performance of the Seasonal Forecasting of the Asian Summer Monsoon by BCC_CSM1.1(m) Advances in Atmospheric Sciences 32:1156-1172 doi:10.1007/s00376-015-4194-8

Liu Y, Liu Z, Zhang S, Rong X, Jacob R, Wu S, Lu F (2004) Ensemble-based parameter estimation in a coupled GCM using the adaptive spatial average method Journal of Climate 27:4002–4014

Lorenc A (1986) Analysis methods for numerical weather prediction Quarterly Journal of the Royal Meteorological Society 112:1177-1194

Luo JJ, Masson S, Behera S, Shingu S, Yamagata T (2005) Seasonal climate predictability in a coupled OAGCM using a different approach for ensemble forecasts Journal of Climate 18:4474-4497 doi:Doi 10.1175/Jcli3526.1

Luo JJ, Masson S, Behera SK, Yamagata T (2008) Extended ENSO predictions using a fully coupled ocean-atmosphere model Journal of Climate 21:84-93 doi:10.1175/2007jcli1412.1

McPhaden MJ (1995) The Tropical Atmosphere Ocean (TAO) array is completed Bulletin of the American Meteorological Society 76:739-741 doi:https://doi.org/10.1029/ 97JC02906.

Molteni F et al. (2011) The new ECMWF seasonal forecast system (System 4) ECMWF Technical Memorandum 656:49pp

Moore AM, Kleeman R (1996) The dynamics of error growth and predictability in a coupled model of ENSO Quarterly Journal of the Royal Meteorological Society 122:1405-1446

Moore AM, Zavala-Garay J, Tang YM, al. e (2006) Optimal forcing patterns for coupled models of ENSO Journal of Climate 19:4683-4699

Nur'utami MN, Hidayat R (2016) Influences of IOD and ENSO to Indonesian Rainfall Variability: Role of Atmosphere-ocean Interaction in the Indo-pacific Sector Procedia Environmental Sciences 33:196-203 doi:10.1016/j.proenv.2016.03.070

Ren H-L, Nie Y (2020) Skillful prediction of winter Arctic Oscillation from previous summer in a linear empirical model Science China Earth Sciences doi:10.1007/s11430-020-9665-3

Ren H-L, Zuo J, Deng Y (2018) Statistical predictability of Niño indices for two types of ENSO Climate Dynamics 52:5361-5382 doi:10.1007/s00382-018-4453-3

Roeckner E, Bäuml G, Bonaventura L, Brokopf R (2003) The atmospheric general circulation model ECHAM5. PART I: Model description Report 349, Max Planck Institute for Meteorology:140pp

Rong XY, Li J, Chen HM, Su JZ, Hua LJ, Zhang ZQ, Xin YF (2020) The CMIP6 Historical Simulation Datasets Produced by the Climate System Model CAMS-CSM Advances in Atmospheric Sciences doi:10.1007/s00376-020-0171-y

Rong XY et al. (2018) The CAMS Climate System Model and a Basic Evaluation of Its Climatology and Climate Variability Simulation Journal of Meteorological Research 32:839-861 doi:10.1007/s13351-018-8058-x

Saha S et al. (2006) The NCEP Climate Forecast System Journal of Climate 19:3483-3517 doi:Doi 10.1175/Jcli3812.1

Shi H, Wang B (2018) How does the Asian summer precipitation-ENSO relationship change over the past 544 years? Climate Dynamics 52:4583-4598 doi:10.1007/s00382-018-4392-z

Small RJ et al. (2014) A new synoptic scale resolving global climate simulation using the Community Earth System Model Journal of Advances in Modeling Earth Systems 6:1065-1094 doi:10.1002/2014ms000363

Su J, Zhang R, Rong X, Min Q, Zhu C (2018) Sea Surface Temperature in the Subtropical Pacific Boosted the 2015 El Niño and Hindered the 2016 La Niña Journal of Climate 31:877-893 doi:10.1175/jcli-d-17-0379.1

Sugiura N et al. (2008) Development of a four-dimensional variational coupled data assimilation system for enhanced analysis and prediction of seasonal to interannual climate variations Journal of Geophysical Research 113 doi:10.1029/2008jc004741

Tang Y, Kleeman R, Moore AM, Weaver A, Vialard J (2003) The use of ocean reanalysis products to initialize ENSO predictions Geophysical Research Letters 30 doi:10.1029/2003gl017664

Tang Y, Lin H, Moore AM (2008) Measuring the potential predictability of ensemble climate predictions Journal of Geophysical Research 113 doi:10.1029/2007jd008804

Tang Y et al. (2018) Progress in ENSO prediction and predictability study National Science Review 5:826-839 doi:10.1093/nsr/nwy105

Tao W, Huang G, Hu K, Gong H, Wen G, Liu L (2015) A study of biases in simulation of the Indian Ocean basin mode and its capacitor effect in CMIP3/CMIP5 models Climate Dynamics 46:205-226 doi:10.1007/s00382-015-2579-0

Wang B, Wu R, Fu X (2000) Pacific−East Asian Teleconnection: How Does ENSO Affect East Asian Climate? Journal of Climate 13:1517-1536 doi:10.1175/1520-0442(2000)013<1517:Peathd>2.0.Co;2

Wang Y et al. (2019) Seasonal predictions initialised by assimilating sea surface temperature observations with the EnKF Climate Dynamics 53:5777-5797 doi:10.1007/s00382-019-04897-9

Winton M (2000) A reformulated three-layer sea ice model Journal of Atmospheric and Oceanic Technology 17:525-531 doi:Doi 10.1175/1520-0426(2000)017<0525:Artlsi>2.0.Co;2

Wu B, Zhou T, Li T (2009) Seasonally Evolving Dominant Interannual Variability Modes of East Asian Climate* Journal of Climate 22:2992-3005 doi:10.1175/2008jcli2710.1

Wu R, Kirtman BP (2003) On the impacts of the Indian summer monsoon on ENSO in a coupled GCM Quarterly Journal of the Royal Meteorological Society 129:3439-3468 doi:10.1256/qj.02.214

Xie S-P, Hu K, Hafner J, Tokinaga H, Du Y, Huang G, Sampe T (2009) Indian Ocean Capacitor Effect on Indo–Western Pacific Climate during the Summer following El Niño Journal of Climate 22:730-747 doi:10.1175/2008jcli2544.1

Xu Q, Guan Z (2017) Interannual variability of summertime outgoing longwave radiation over the Maritime Continent in relation to East Asian summer monsoon anomalies Journal of Meteorological Research 31:665-677 doi:10.1007/s13351-017-6178-3

Xue Y, Cane MA, Zebiak SE, Blumenthal MB (1994) On the prediction of ENSO: a study with a low-order Markov model Tellus A: Dynamic Meteorology and Oceanography 46:512-528 doi:10.3402/tellusa.v46i4.15641

Yang J, Liu Q, Xie S-P, Liu Z, Wu L (2007) Impact of the Indian Ocean SST basin mode on the Asian summer monsoon Geophysical Research Letters 34 doi:10.1029/2006gl028571

Yu RC (1994) A two-step shape-preserving advection scheme Advances in Atmospheric Sciences 11:479-490

Zhang H, Shi GY, Nakajima T, Suzuki T (2006a) The effects of the choice of the k-interval number on radiative calculations Journal of Quantitative Spectroscopy & Radiative Transfer 98:31-43 doi:10.1016/j.jqsrt.2005.05.090

Zhang H, Suzuki T, Nakajima T, Shi GY, Zhang XY, Liu Y (2006b) Effects of band division on radiative calculations Optical Engineering 45 doi:Artn 016002

10.1117/1.2160521

Zhang R, Sumi A, Kimoto M (1999) A diagnostic study of the impact of El Niño on the precipitation in China Advances in Atmospheric Sciences 16:229-241 doi:10.1007/bf02973084

Zhang S, Harrison M, Rosati A, Wittenberg A (2007) System design and evaluation of coupled ensemble data assimilation for global oceanic climate studies Monthly Weather Review 133:3176–3201

Zhong W, Cai W, Zheng XT, Yang S (2019) Unusual Anomaly Pattern of the 2015/2016 Extreme El Niño Induced by the 2014 Warm Condition Geophysical Research Letters 46:14772-14781 doi:10.1029/2019gl085681

Zhu J, Kumar A, Lee H-C, Wang H (2017) Seasonal predictions using a simple ocean initialization scheme Climate Dynamics 49:3989-4007 doi:10.1007/s00382-017-3556-6

Figures
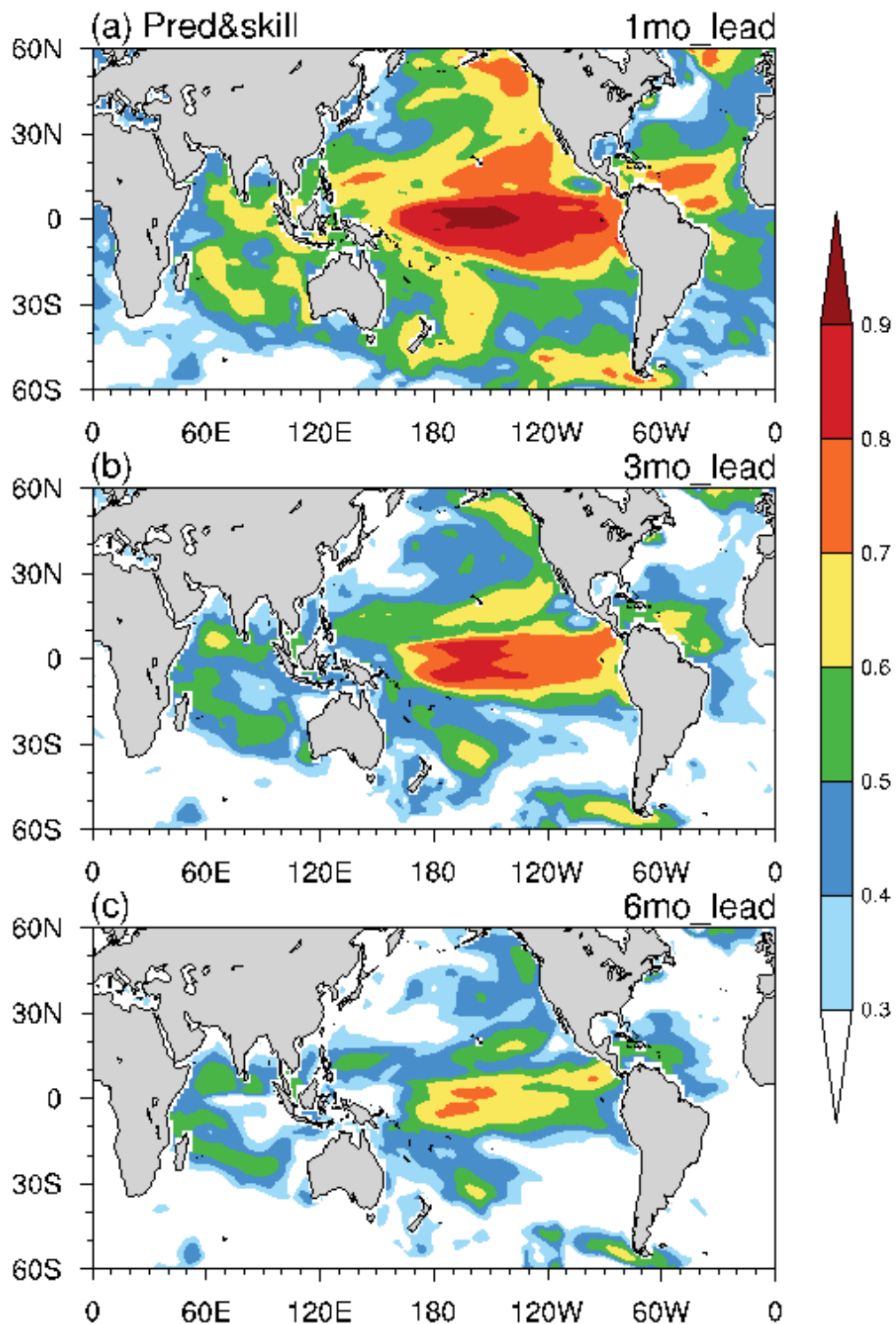
Figure 1

Distribution of correlation between the observed and predicted SST anomalies at 1- (a), 3- (b), and 6-month (c) lead times during 1981-2019. All shading areas are above 90% confidence level (correlation of 0.26 is 90% confidence level according to Student's t test with the degree of freedom of 38). Note: The designations employed and the presentation of the material on this map do not imply the expression of any opinion whatsoever on the part of Research Square concerning the legal status of any country, territory, city or area or of its authorities, or concerning the delimitation of its frontiers or boundaries. This map has been provided by the authors.
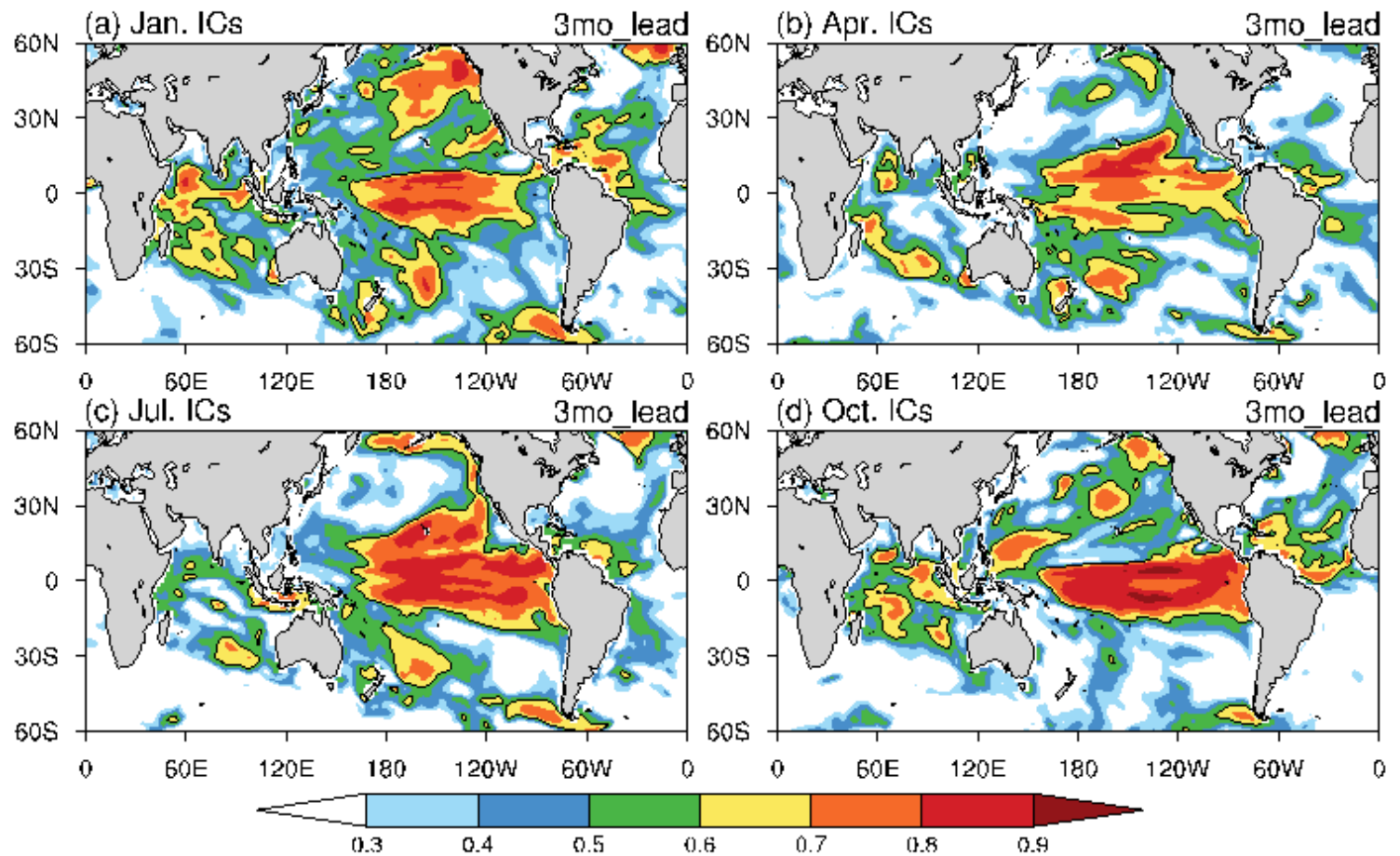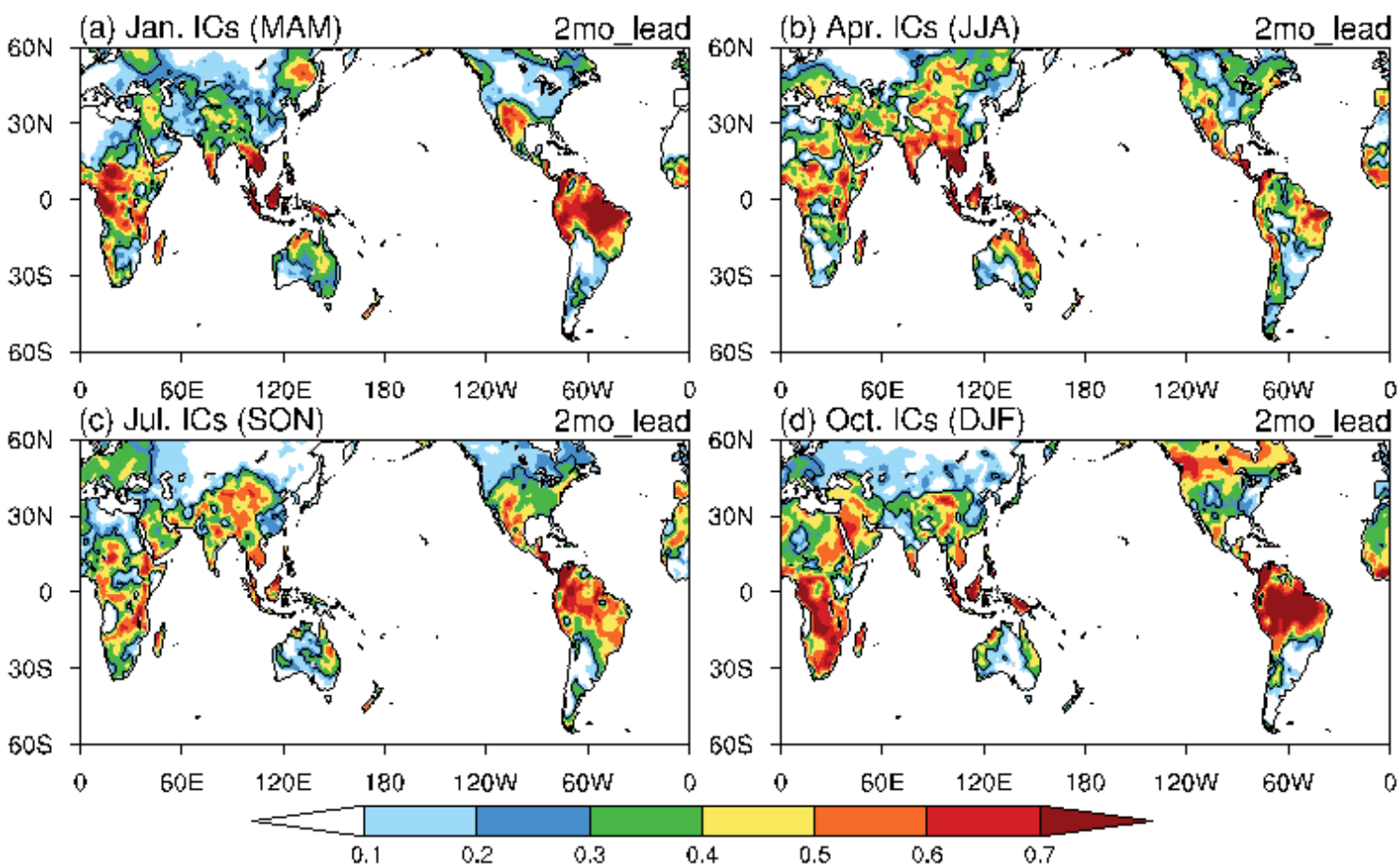
Figure 2

Distribution of correlations between the observed SST anomalies and the predicted values at 3-month lead time with initial time starting from January (a), April (b), July (c) and October (d) during 1981-2019. All shaded areas are above 90% confidence level. Contour lines indicate the ACC of 0.6. Note: The designations employed and the presentation of the material on this map do not imply the expression of any opinion whatsoever on the part of Research Square concerning the legal status of any country, territory, city or area or of its authorities, or concerning the delimitation of its frontiers or boundaries. This map has been provided by the authors.
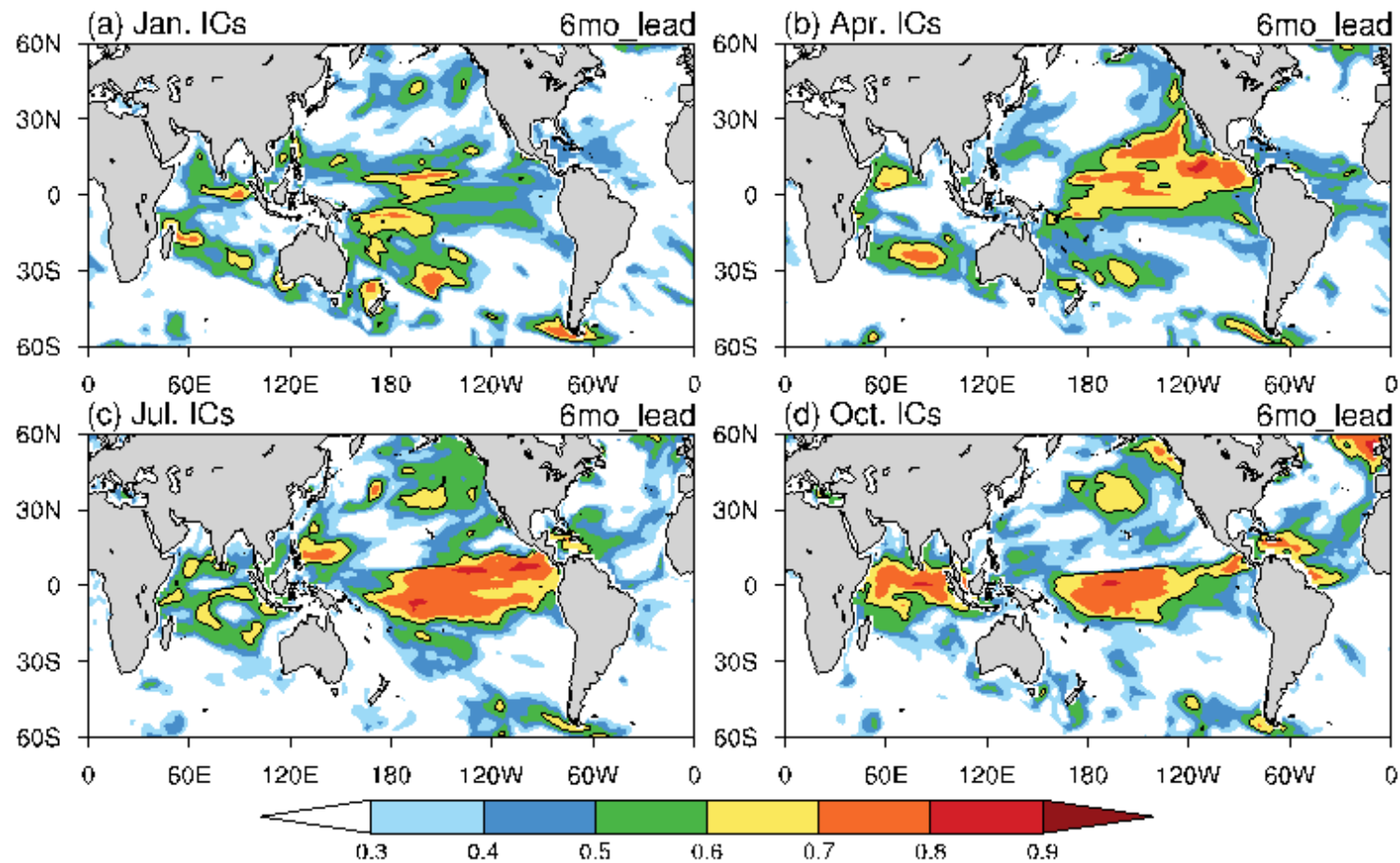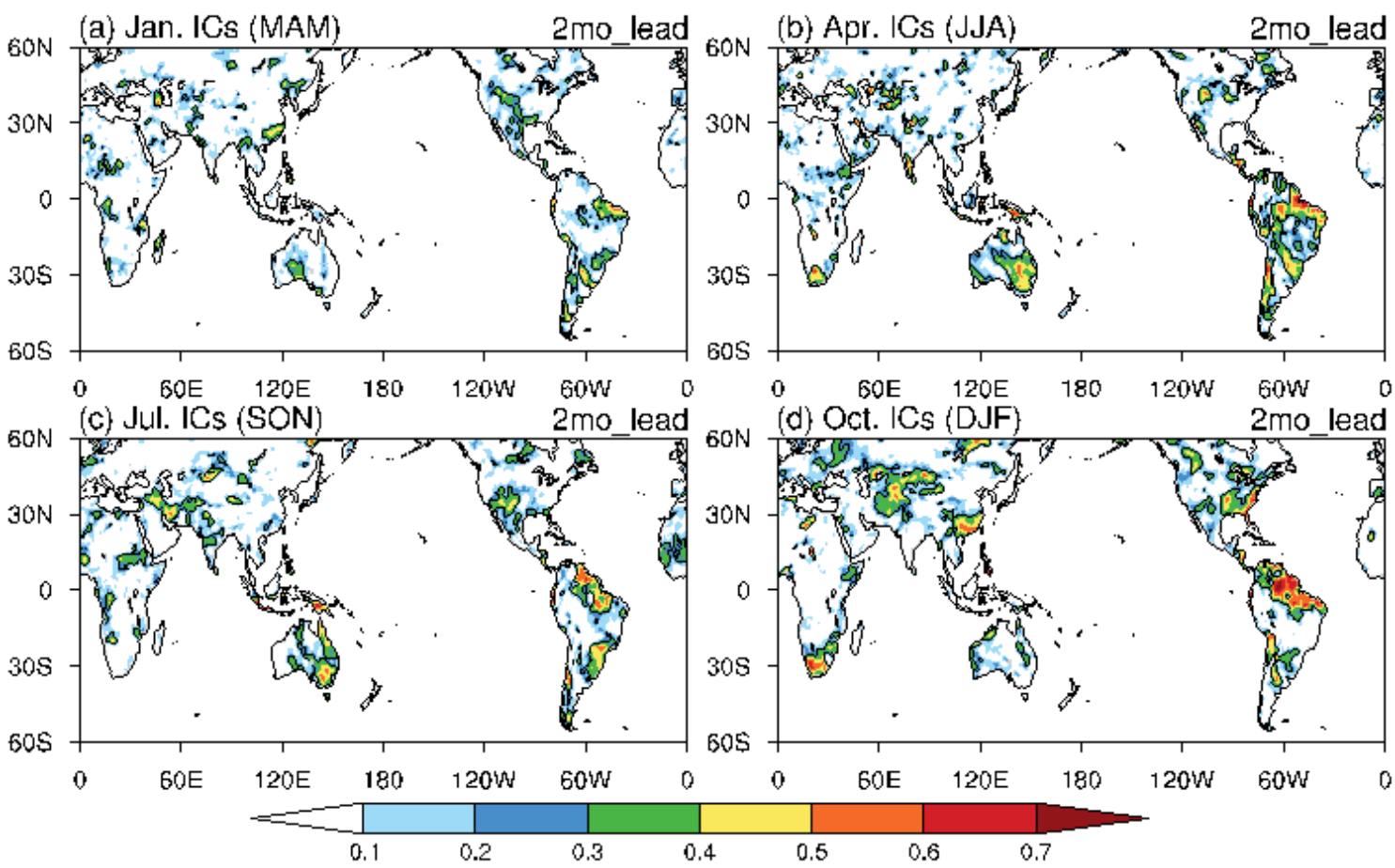
Figure 3

Same as Fig. 2 but for 6-month lead time. Note: The designations employed and the presentation of the material on this map do not imply the expression of any opinion whatsoever on the part of Research Square concerning the legal status of any country, territory, city or area or of its authorities, or concerning the delimitation of its frontiers or boundaries. This map has been provided by the authors.
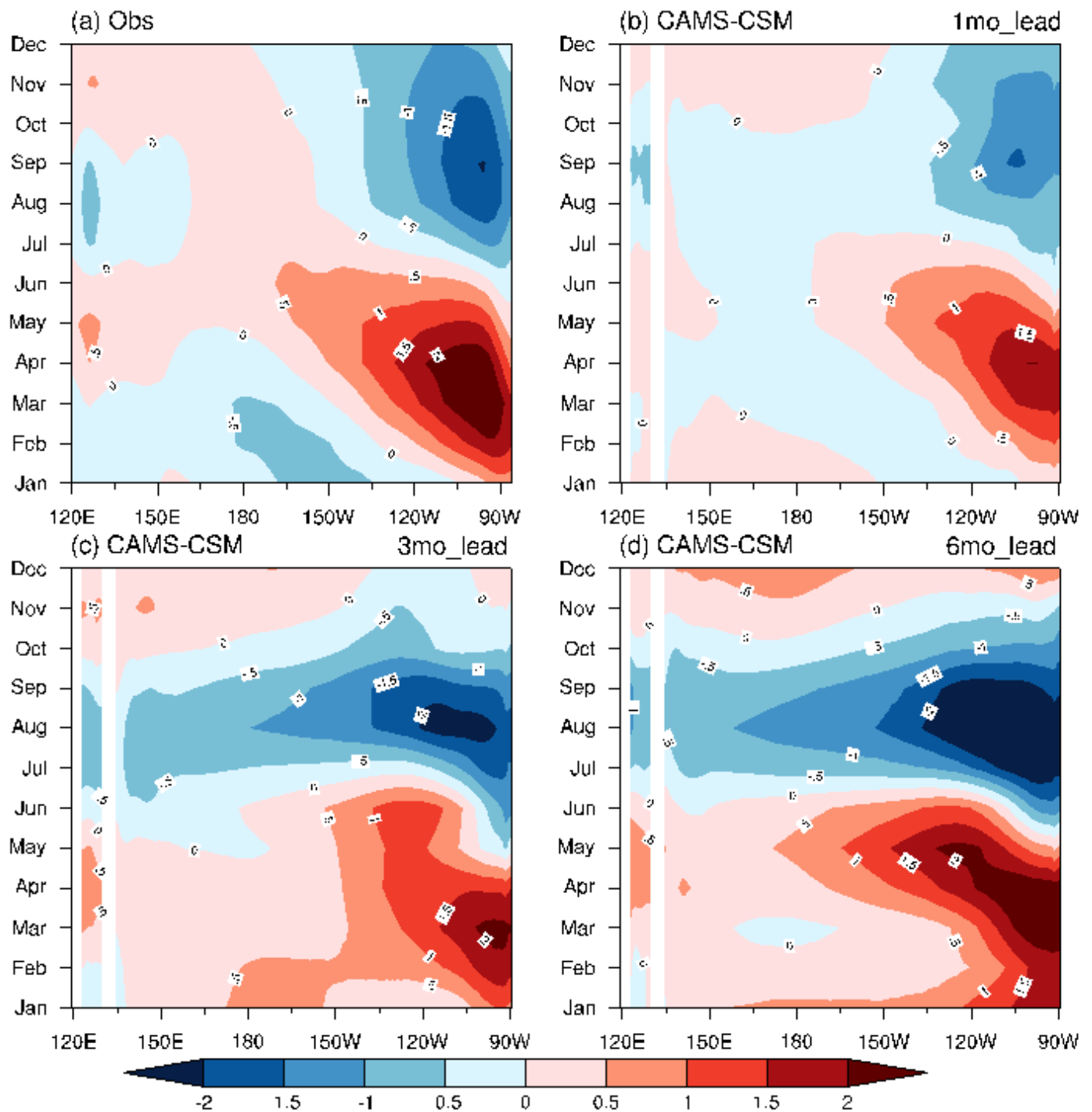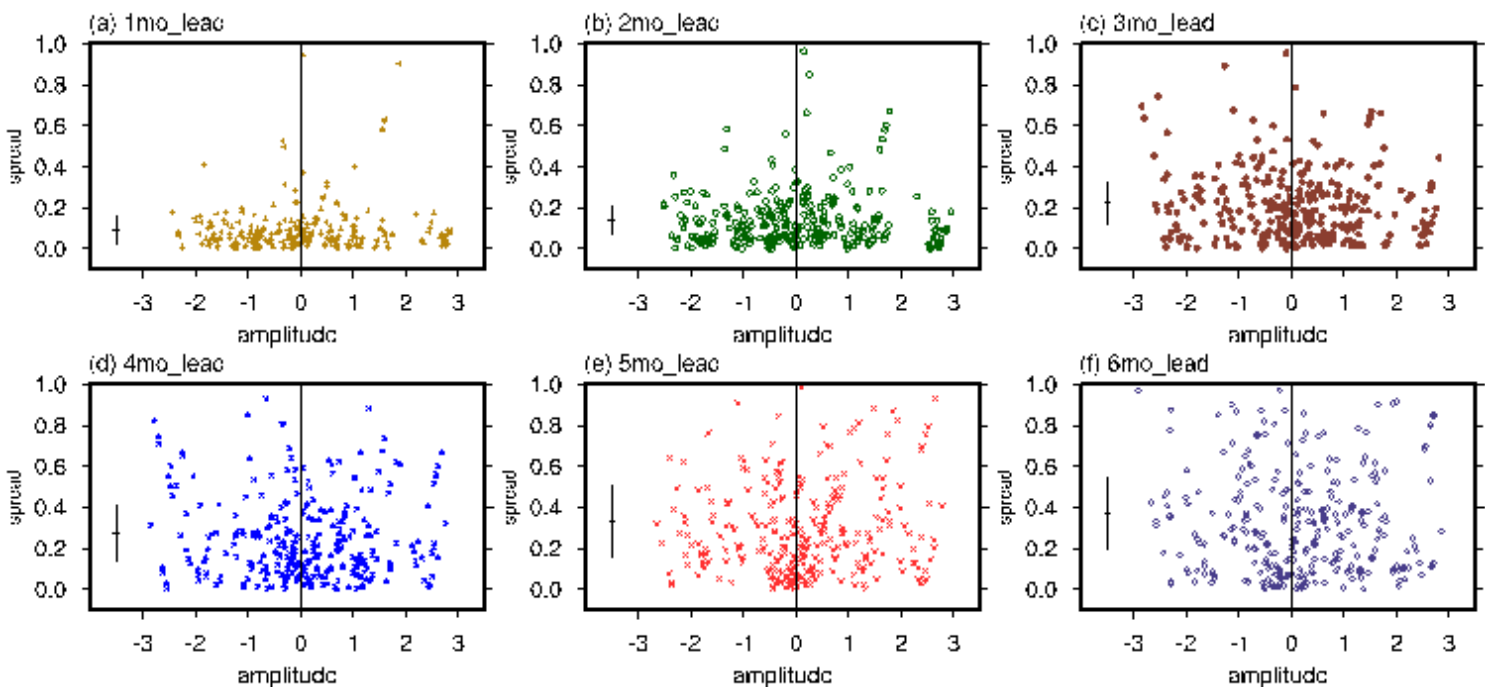

Figure 4

Same as Fig. 2 but for seasonal 2-m air temperature anomalies at 2-month lead time. Contour is 0.26 which is significant at 90% level. Note: The designations employed and the presentation of the material on this map do not imply the expression of any opinion whatsoever on the part of Research Square concerning the legal status of any country, territory, city or area or of its authorities, or concerning the delimitation of its frontiers or boundaries. This map has been provided by the authors.

Figure 5

Same as Fig. 4 but for seasonal precipitation. Note: The designations employed and the presentation of the material on this map do not imply the expression of any opinion whatsoever on the part of Research Square concerning the legal status of any country, territory, city or area or of its authorities, or concerning the delimitation of its frontiers or boundaries. This map has been provided by the authors.

Figure 6

The seasonal cycle of the tropical Pacific SST deviation from the annual mean in the (a) observation and prediction at (b) 1-, (c) 3- and (d) 6-month lead time, respectively. Note: The designations employed and

Figure 7

Scatterplots of the DJF Niño3.4 SST index against the ensemble spread in CAMS-CSM hindcasts at (a) 1-, (b) 2-, (c) 3-, (d) 4-, (e) 5-, (f) 6-month lead time, respectively. The x axis is for the ensemble mean of 3-

month-mean predictions and the y axis is the spread of the 8 members. Different lead times are displayed by different colors and shapes. The average and standard deviation of the spread at each lead time are shown in an error-bar form (thick black line in bottom left), which the vertical length represents the standard deviation and its center point corresponds to the value on the y-axis represents the average spread. The unit is °C.
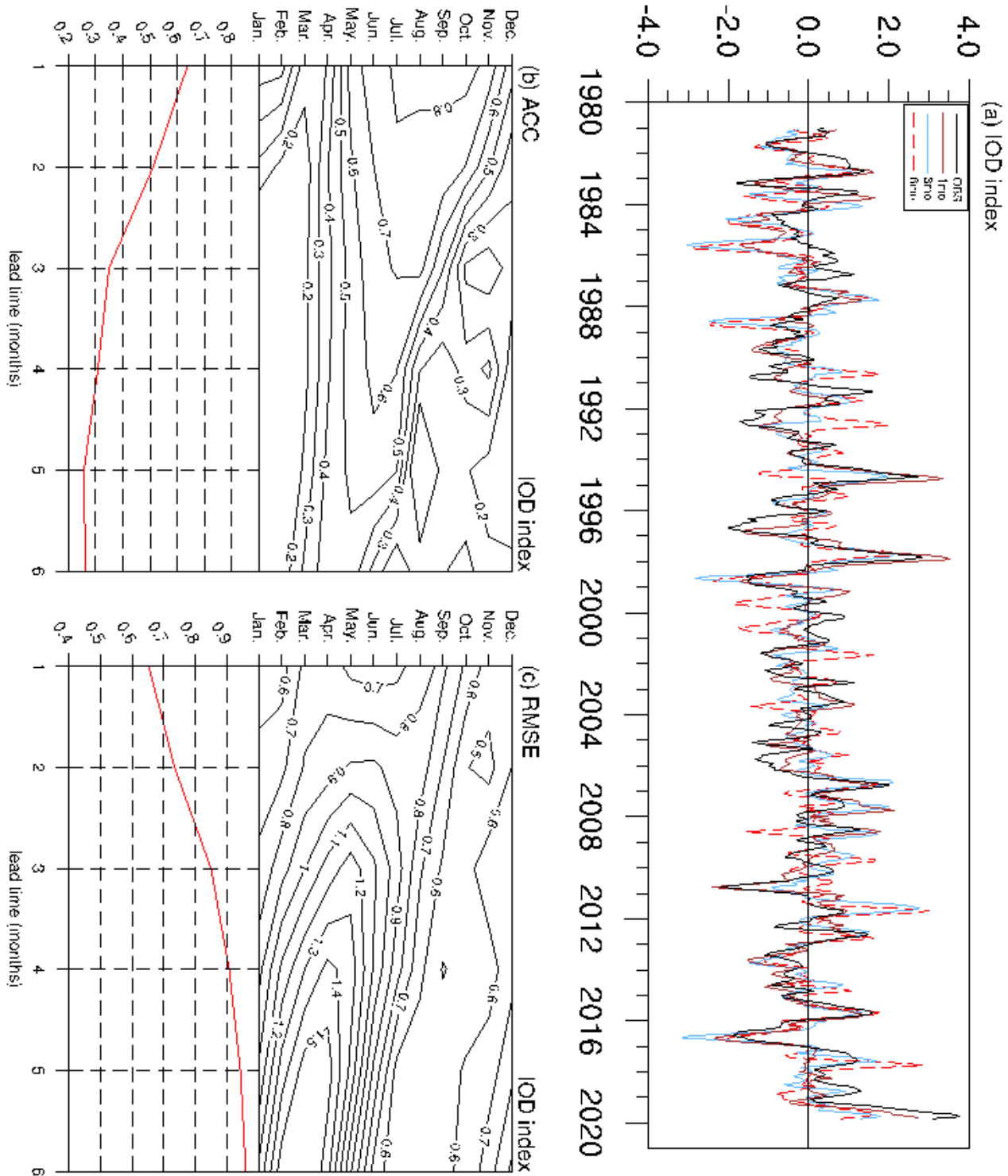

Figure 8
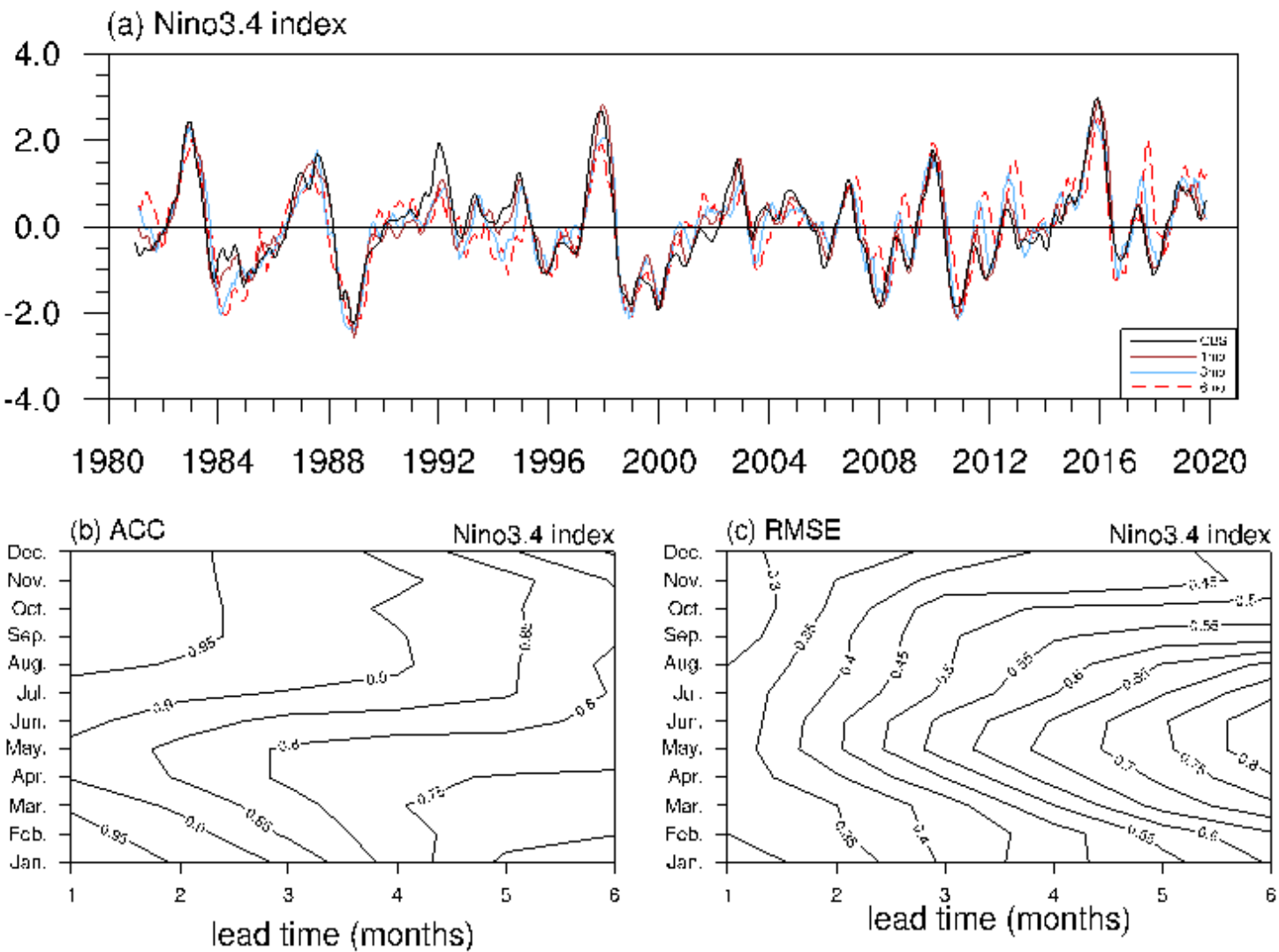
(a) The Niño3.4 index [area-averaged SSTA 5°S-5°N, 170°-120°W] based on the ERSSTv5 observations (solid red line) and model ensemble mean predictions at 1- (blue line), 3- (brown line) and 6-month (green line) lead time during 1981-2019. The (b) ACC and (c) RMSE of the Niño3.4 index predictions as a function of lead time and different calendar months.
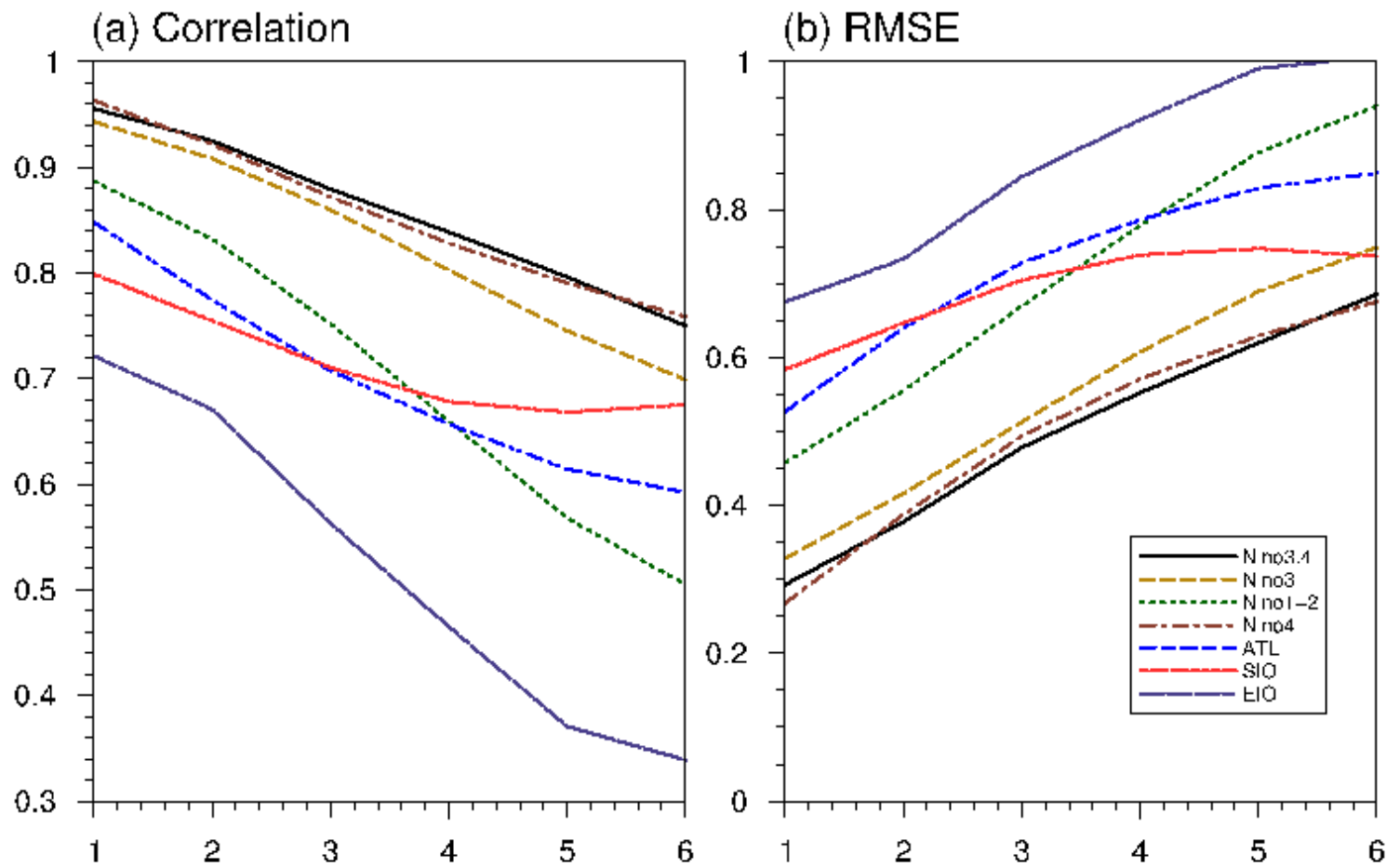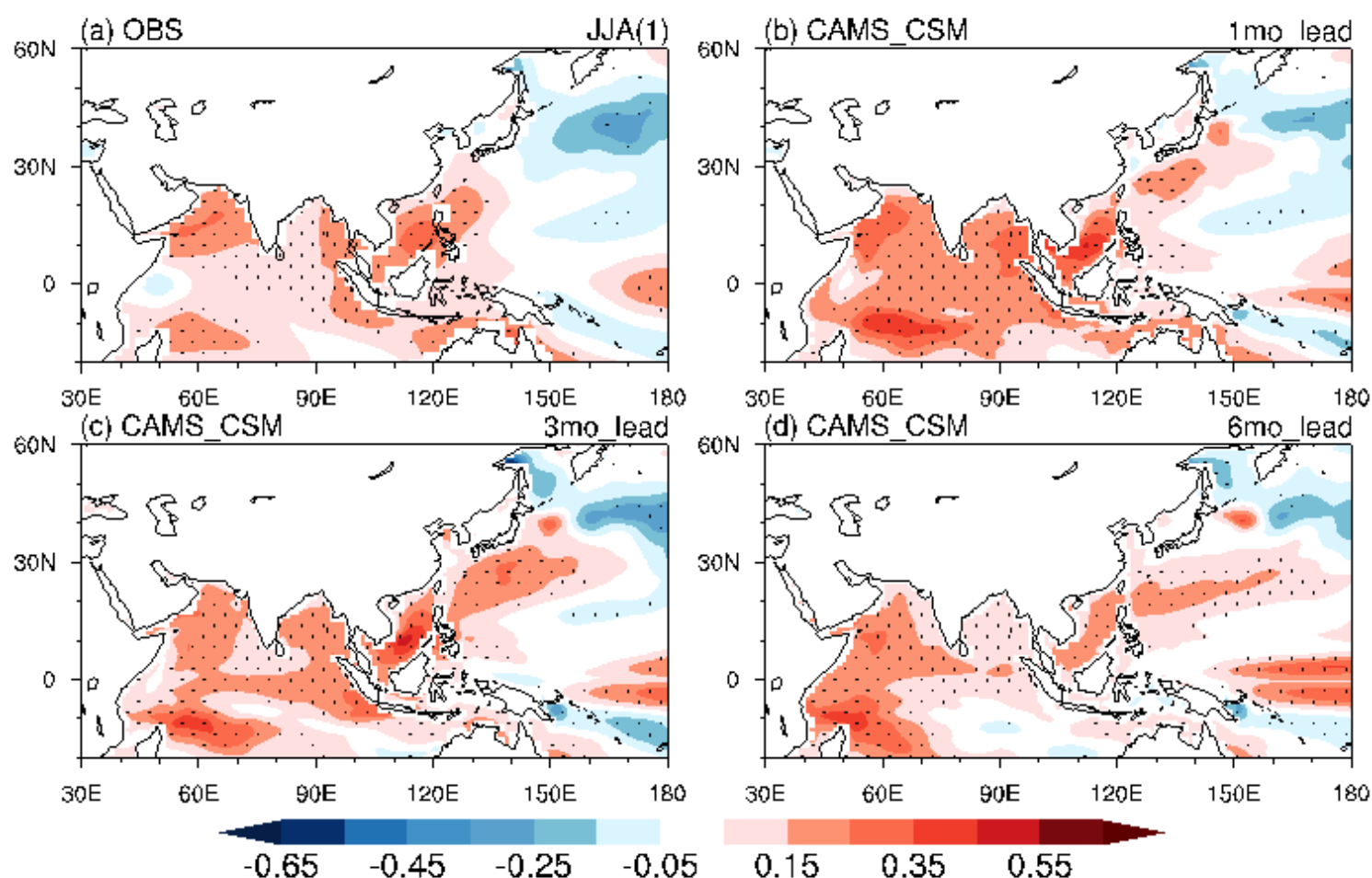

Figure 9

The ACC (a) and RMSE (b) of Niño3.4, Niño3 [5S-5N, 150W-90W],Niño1+2 [-10S-0, 90W-80W], Niño4 [5S-5N, 160E-150W], ATL[10N-20N, 40E-60E], South Indian Ocean [SIO, 20S-10S, 50-70], and eastern Indian

Ocean [EIO, 10S-0,90W-110W] indexes as a function of forecast lead months (x-axis) for each month. All the above indexes are calculated by model ensemble mean SSTA area-averaged in the range within square brackets.
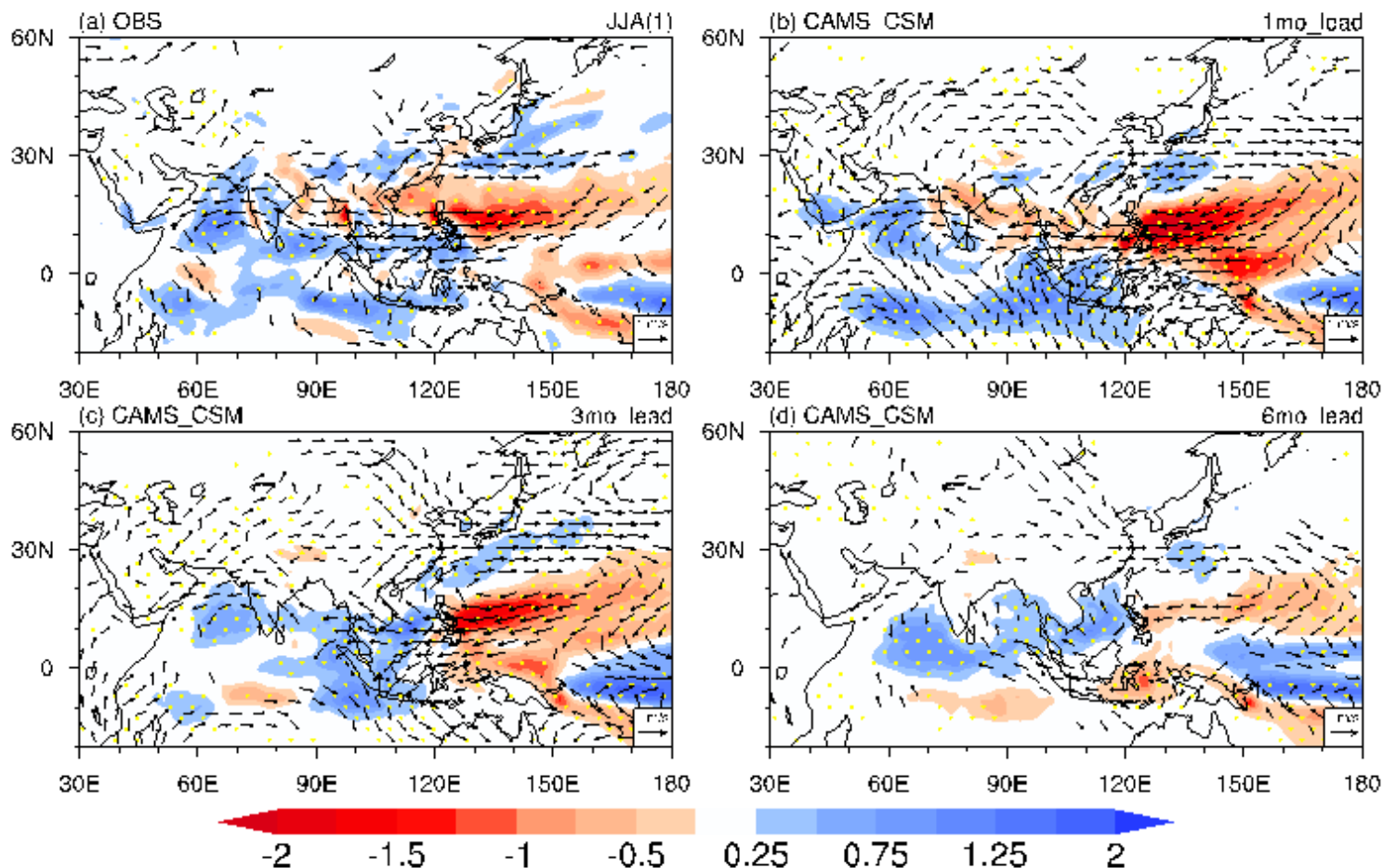

Figure 10

Same as Fig. 8 but for IOD index, corresponding with the total annual mean below. The IOD index is area-averaged SSTA difference between the tropical western Indian Ocean (10°S-10°N, 50°-70°E) and the tropical southern Indian Ocean (10°S-0°, 90°-110°E).

Figure 11

The regression of JJA(1) SST anomalies in the observation (a) and model ensemble mean predicted at 1- (b), 3- (c) and 6-month (d) lead time with DJF(0) Niño3.4 index. The areas where significance above 90% are dotted. Note: The designations employed and the presentation of the material on this map do not imply the expression of any opinion whatsoever on the part of Research Square concerning the legal status of any country, territory, city or area or of its authorities, or concerning the delimitation of its frontiers or boundaries. This map has been provided by the authors.

Figure 12

The regression of JJA(1) precipitation anomalies in the observation (a) and model ensemble mean predicted at 1- (b), 3- (c) and 6-month (d) lead time with DJF(0) Niño3.4 index. The areas where significant above 90% are dotted. The wind is shown when the zonal or meridional components is significant at 10% level using Student's t test. Note: The designations employed and the presentation of the material on this map do not imply the expression of any opinion whatsoever on the part of Research

Square concerning the legal status of any country, territory, city or area or of its authorities, or concerning the delimitation of its frontiers or boundaries. This map has been provided by the authors.